DC and AC Characterization of MgO Magnetic Tunnel Junction Sensors

Mustafa Arikan[1], Snorri Ingvarsson[1], Matthew Carter[2], and Gang Xiao[3]

[1]Science Institute, University of Iceland, Reykjavik IS-107, Iceland
[2]Micromagnetics Inc., Fall River, MA 02720 USA
[3]Physics Department, Brown University, Providence, RI 02912 USA

We have fabricated multiple MgO magnetic tunnel junctions (MTJ) with 1.7 nm oxide, which are connected in series, and layed out in a serpentine geometry. We performed DC tunnel magnetoresistance measurements and AC impedance spectroscopy with crossed DC magnetic fields in the easy and hard axis directions. A simple RLC circuit model is used to fit our data and characterize the dependence on capacitance (C) and inductance (L) of magnetization orientation of the MTJ sensors. We have found in our samples that C and L are higher in antiparallel than in parallel configuration. We discuss possible reasons for the existence of this field dependence and show the evolution of magnetic field vs. capacitance curve from memory mode into sensing mode at high frequencies.

***Index Terms*—Magnetic sensors, magnetic tunnel junction, magnetocapacitance, magnetoimpedance, magnetoinductance, magnetoresistance, MgO.**

I. Introduction

MAGNETIC TUNNEL JUNCTIONS (MTJs) are among the most successful devices in spintronics. They are used in many applications such as magnetoresistive random access memory, in read heads for magnetic media, magnetic field sensors and magnetic microscopy [1]–[3]. With the introduction of magnesium oxide (MgO), tunnel magnetoresistance (TMR) has increased to values as high as 600% at room temperature [4]. Recently, there has been a growing interest in AC response of the MTJs since it is crucial to understand AC characteristics of the MTJs in order to study various important spin effects such as frequency-dependent spin transport, spin capacitance and electron-electron interactions in spintronic devices [5]–[7]. AC magnetotransport has also been proposed as a useful tool to probe spin dependent potentials, dielectric relaxation mechanisms and high frequency magnetic sensing [8]–[12]. Previous studies found in the literature focus on large area single tunnel junctions ($\geq 1000\ \mu\mathrm{m}^2$) with Al-oxide and a few with MgO as the insulator.

If the magnetic moments of ferromagnetic electrodes in a tunnel junction are aligned along the same axis, either parallel or antiparallel, then resistance vs. applied field curve $(R(H))$ will be hysteretic (multivalued function). The magnetic moment of the free layer will rotate abruptly with respect to the external field, resulting in a jump in the resistance of the tunnel junction due to switching between parallel (P) and anti-parallel (AP) alignment of the magnetization. In this case the tunnel junction is said to be in the memory (or switching) mode. One, however, needs a single-valued function in order to be able to use the MTJs as a magnetic field sensor. Ideally, the $R(H)$ curve must be a non-hysteretic curve with zero coercivity and it should show a steep slope (dR/dH) in the sensing regime. This configuration is known as the sensing-mode. It can be achieved with the help of shape anisotropy by fabricating the junctions as ellipses [13], [14] or orienting the magnetization vector of the free layer out of plane due to the perperdicular magnetic anisotropy of the MgO/CoFeB interface [15], [16].

Another way to drive the junctions into this configuration is to apply a DC field along the hard axes of the ferromagnetic electrodes. The hard axis field will rotate the magnetic moment of the free layer perpendicular to the pinned layer and the MTJ will be in sensing mode. Also, it has recently been reported that it is possible to fabricate MTJ sensors with a superparamagnetic free layer [17].

In this report, we present our results of DC and AC characterization of unbiased MgO MTJ sensors. A simple RLC circuit model was used to fit the frequency dependent impedance data. We use the results to show the evolution of spin capacitance as the applied field in hard axis direction increases.

II. Experiment

Each of the 6 sensors used in this work have 24 to 65 identical MTJs with 1.7 nm MgO insulator. The individual junctions with an area of 6.28 $\mu\mathrm{m}^2$ were placed in a serpentine geometry in order to minimize the total sensor area and connected to each other in series to obtain higher resistance and robustness (Fig. 1: inset). The individual MTJs have the following structure (thicknesses in nm): $\mathrm{Ta(30)/Co_{50}Fe_{50}(3)IrMn(15)/Co_{50}Fe_{50}(2)/Ru(0.8)/Co_{40}Fe_{40}B_{20}(3)/MgO(1.7)/Co_{40}Fe_{40}B_{20}(30)/Ta(10)/Ru(5)}$. The layers were deposited by magnetron sputtering onto a thermally oxidized Si wafer. An artificial antiferromagnet stack (CoFe/Ru/CoFeB) was deposited in order to increase the exchange bias and enhance the thermal stability as well as forming a barrier to prevent Mn diffusion from IrMn into MgO layer at high temperatures. Post-processing thermal annealing was then performed in vacuum at a temperature of 375°C for 1 h with an applied field of 2.5 kOe. We refer to Liu *et al.* [18] for the detailed description of the fabrication process and optimized parameters. We report the measurements of 6 devices (S1–S6) which include different number of individual junctions between 24 and 65.

Manuscript received March 24, 2013; revised May 11, 2013; accepted May 24, 2013. Date of publication June 06, 2013; date of current version October 21, 2013. Corresponding author: M. Arikan (e-mail: mua1@hi.is).

Color versions of one or more of the figures in this paper are available online at http://ieeexplore.ieee.org.

Digital Object Identifier 10.1109/TMAG.2013.2266327

0018-9464 © 2013 IEEE

Authorized licensed use limited to: Brown University. Downloaded on March 24,2023 at 17:51:20 UTC from IEEE Xplore. Restrictions apply.

TABLE I
DC-MAGNETORESISTANCE MEASUREMENTS UNDER ZERO HARD AXIS FIELD. ANTIPARALLEL AND PARALLEL RESISTANCE VALUES WERE MEASURED AT ±40 OE EASY AXIS FIELDS. EVEN THOUGH THE SENSORS ARE NOT LISTED IN ORDER OF INCREASING NUMBER OF JUNCTIONS, THERE IS A LINEAR INCREASE IN R WITH THE NUMBER OF INDIVIDUAL JUNCTIONS

Device	No. Individual junctions	R_{ap} (Ω)	R_{p} (Ω)	TMR (%)
S1	24	1086	573	89.5
S2	32	2045	849	140.9
S3	65	11335	4951	128.9
S4	24	922	466	97.9
S5	24	1240	564	119.9
S6	38	4540	2055	120.9

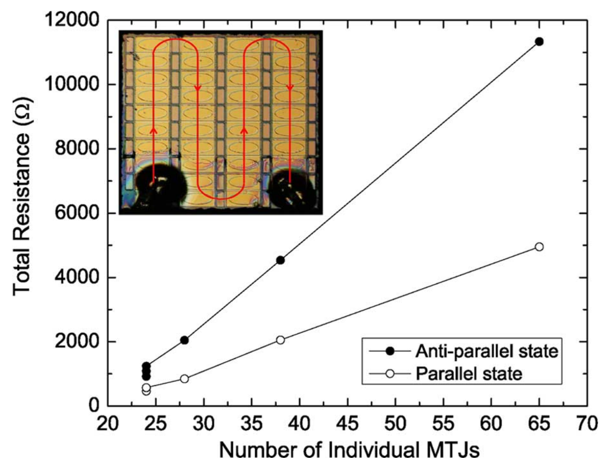

Fig. 1. Total sensor resistance vs. number of individual MTJs. Inset: Microscope picture of a similar device used in this work. The red line indicates the path of the current across the device. The current weaves its way into and out of the plane through the successive junctions.

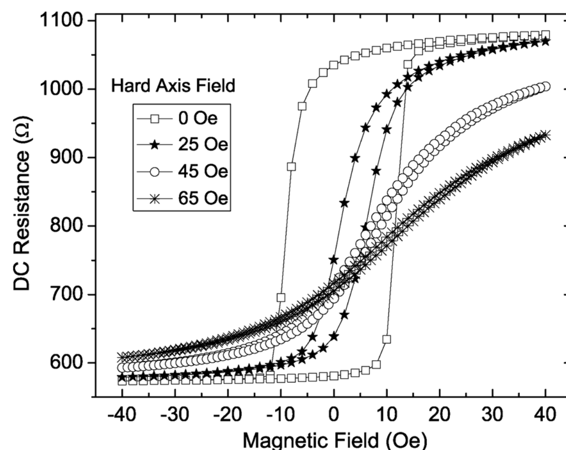

Fig. 2. DC magnetoresistance vs. easy axis field under constant external fields (0, 25, 45 and 65 Oe) along the hard axis.

We performed DC magnetoresistance measurements and AC impedance spectroscopy of the MTJ sensors under an external magnetic field along the easy axis of the MTJs, which was swept between ±40 Oe in 1 Oe steps. During each sweep, second external magnetic field was applied along the hard axis in 5 Oe steps between 0–65 Oe in order to drive the MTJs gradually from memory-mode to sensor-mode. This allowed us to observe the evolution of the spin dependent impedance of the MTJs under an external hard axis field. DC-resistance measurements were performed with a Keithley 2400 source meter by standard 4-wire configuration with 100 mV constant applied voltage. AC impedance spectroscopy measurements were performed between 100 Hz and 40 MHz by using HP 4194A impedance analyzer with a HP 16085B measurement fixture. A 100 mV AC signal was applied in 4-probe configuration. All the measurements were repeated using HP 4284A LCR meter to prove that the results are repeatable and independent of the experimental setup. We followed standard calibration procedures (short, open, load) before each measurement to cancel the contribution of cables and leads as well as the effect of magnetic fields on the connections. By using standard components (resistors, capacitors and inductors), several complex RLC circuits were constructed and measured in order to find out our measurements' sensitivity, in particular to small capacitances, as our devices have small capacitance. We were able to measure capacitance values down to 0.06 pF reliably.

III. MEASUREMENTS & RESULTS

Six devices (S1–S6) were characterized in total. The total resistance of the sensors increases linearly with the number of individual junctions (Fig. 1 and Table I). The slope for the parallel and anti-parallel states is different because of varying TMR ratios for each sensor. Fig. 2 shows the magnetoresistance measurements for the MTJ sensor-1 (S1). $R(H)$ curves are shown for different external fields which were applied in the hard axis direction and kept constant during the measurement for each loop while the sweeping field was applied along the easy axis. We show only 4 curves out of 14 for clarity. DC-TMR values were found by the traditional definition: $100 \times (R_{\rm ap} - R_{\rm p})/R_{\rm p}$, where $R_{\rm ap}$ $(R_{\rm p})$ is the resistance of the antiparallel (parallel) magnetization state. TMR for S1 is 89.5% $(R_{\rm ap} = 1086\ \Omega, R_{\rm p} = 573\ \Omega)$ for zero hard axis field and it reduces to 53.5% $(R_{\rm ap} = 932\ \Omega, R_{\rm p} = 607\ \Omega)$ as the hard axis field is increased to 65 Oe which is shown in Fig. 3. The resistance of the sensor in the parallel state increases from 573 to 607 Ω as the hard axis field changes from 0 to 65 Oe with $\Delta R_{\rm p} = 34\ \Omega$ or 5.9%, while the resistance of the anti-parallel state decreases from 1086 to 932 Ω with $\Delta R_{\rm ap} = -154\ \Omega$ or 14.2%. As the hard axis field is increased the coercivity also decreases and the hysteretic $R(H)$ response becomes a single-valued function. The sensitivity is given by the slope of this function in the sensing regime $(1/R \times dR/dH)$. For S1, the coercivity vs. hard axis field is given in Fig. 4. According to the results, the coercivity is ∼20 Oe for 0 Oe hard axis field

Authorized licensed use limited to: Brown University. Downloaded on March 24,2023 at 17:51:20 UTC from IEEE Xplore. Restrictions apply.

TABLE II
MODEL PARAMETERS EXTRACTED FROM DATA, BASED ON EQS. (1) AND (2)

	R_{ap} (Ω)	R_p (Ω)	C_{ap} (pF)	C_p (pF)	L_{ap} (μH)	L_p (μH)
S1	1060	568	5.50	4.95	0.27	0.18
S2	2050	860	6.20	5.70	0.45	0.23
S3	11320	4936	5.80	5.00	0.95	0.64
S4	927	469	5.45	4.85	0.39	0.27
S5	1247	569	5.25	4.95	0.38	0.25
S6	4527	2037	5.00	4.80	0.52	0.34

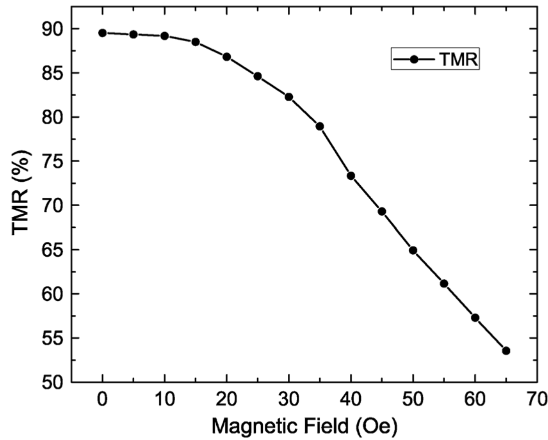

Fig. 3. Tunneling magnetoresistance vs. external field along the hard axis. TMR values were calculated by using R_{p} and R_{ap} at ±40 Oe easy axis fields.

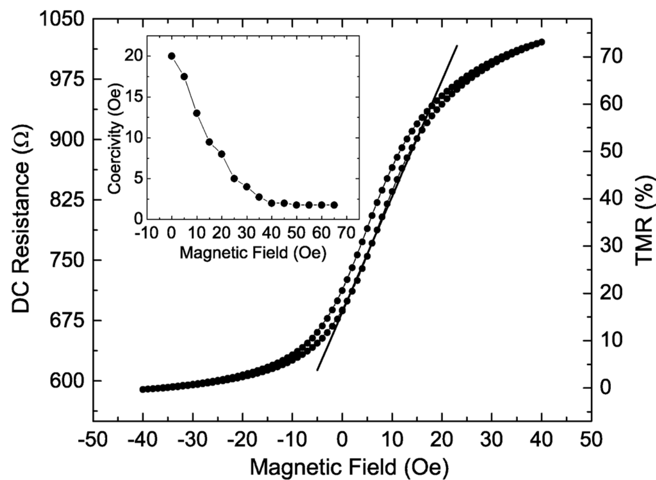

Fig. 4. Linear fit in the sensing regime. The solid line is the fit curve between 0 and 20 Oe. Inset: Coercivity vs. hard axis field.

and it decreases to ~1.75 Oe and saturates at this value as the external field increases to 40 Oe. The sensitivity was found by linear fitting in the sensing regime between 0 and 20 Oe. The results change between $17.8 \times 10^{-3}/\mathrm{Oe}$ and $8.5 \times 10^{-3}/\mathrm{Oe}$ for 40 and 65 Oe hard axis fields, respectively.

We show only one of these $R(H)$ curves and its fit in Fig. 4 for clarity. A summary of DC-magnetoresistance measurements under zero hard axis field is given in Table II. The other devices used in this study (S2–S6) also show similar characteristics with respect to external applied field along the hard axis.

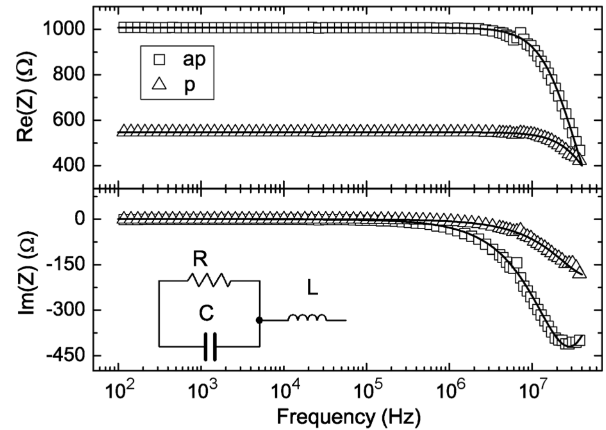

Fig. 5. Real and imaginary impedance as a function of frequency at room temperature for the parallel and antiparallel magnetization configurations. The solid lines are the fit to the data by using the equivalent circuit (inset) as explained in the text. For clarity we have reduced the number of data points.

Using impedance spectroscopy, we evaluated the possibility of using spin capacitance concept in magnetic field sensing once we determined the necessary parameters and conditions to drive the MTJ devices into sensing mode. For the device S1, the frequency dependent impedance for the parallel and anti-parallel states under zero hard axis field are displayed in Fig. 5. The triangles and squares in the figures show the measurement results while the solid lines are fitting curves. A tunnel junction can be modeled as a leaky capacitor. Therefore it can be represented by a complex circuit with resistances and capacitances. Such models are widely accepted and applied in similar works found in the literature, ranging from a simple parallel RC circuit [9], [10] to much more complex RLC models [19]. We have chosen to use a simple circuit model with minimum number of components for our data. As the model becomes more complicated, the number of parameters affecting the impedance increases. Therefore it becomes possible to find several ways to fit the experimental data succesfully by adjusting the values of the components in the model in different combinations. We started with a parallel RC model; a resistor and a capacitor connected in parallel since Cole-Cole plots (not shown here) have semi-circular patterns which is a hint for the existence of parallel RC networks. However, this model didn't capture our data for all the frequency regimes. Also, the exact solutions of this model resulted with frequency dependent TMR and tunnel magneto-capacitance (TMC), especially at high frequencies, which is an indication of the inductive nature of the data. We modified this

Authorized licensed use limited to: Brown University. Downloaded on March 24,2023 at 17:51:20 UTC from IEEE Xplore. Restrictions apply.

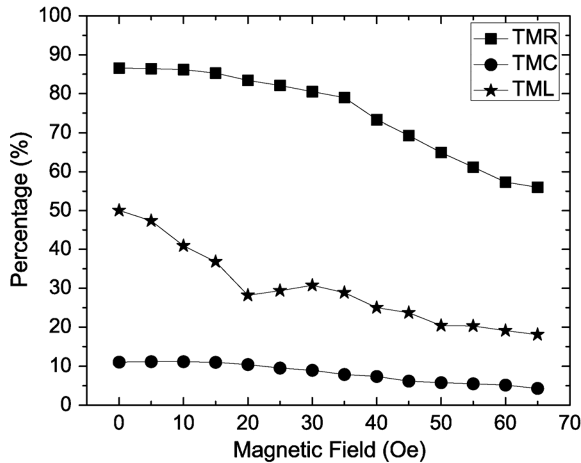

Fig. 6. The TMR, TMC and TML values vs. hard axis field. The values were found by fitting the data to eq. (1) & (2).

TABLE III
MODEL PARAMETERS EXTRACTED FROM DATA FOR ZERO HARD AXIS FIELD, BASED ON EQS. (1) AND (2)

	S1	S2	S3	S4	S5	S6
TMR	86.6	138.4	129.3	97.7	119.2	122.2
TMC	11.1	8.8	16.0	12.4	6.1	4.2
TML	50.0	95.7	48.4	44.4	52.0	52.9

model by adding an inductor in series (Fig. 5) in order to include the effects of the wire bonds and transmission lines in the device. This circuit is modeled by the equations below:

$$\mathrm{Re}(Z) = \frac{R}{1+(\omega RC)^2} \tag{1}$$

$$\mathrm{Im}(Z) = \omega L - \frac{\omega R^2 C}{1+(\omega RC)^2}. \tag{2}$$

For an unknown MTJ, this presents two equations for three unknowns, namely resistance (R), inductance (L), and capacitance (C). However, R can be obtained from the low frequency limit and in our case it agrees well with DC resistance measurements. Then L and C can be determined by fitting (1) and (2) to the data. Using this model we were able to fit our data with frequency independent L and C, and two different R values which correspond to parallel and antiparallel alignment respectively, as seen in Fig. 5 All the parameters are frequency independent, as one hopes to find if such a lumped circuit element model is to faithfully represent the physical system. TMR, TMC and tunnel magnetoinductance (TML) values decreased as we increased hard axis field from 0 to 65 Oe. For S1, the TMR which is 86.6% for zero hard axis field, decreased to 56% for 65 Oe, respectively, as seen in Fig. 6. In a similar fashion, TMC changed from 11.1% to 4.3% while corresponding values were 50% and 18.1% for the TML. The devices S2–S6 showed similar results. The TMR, TMC and TML values under zero hard axis field for all the devices are summarized in Table III.

Since our devices have 24 single MTJs connected in series, the measured capacitance C is not equal to the individual MTJ capacitance C_s but $C_s/24$, assuming they are all identical. Therefore, for S1, the single MTJ capacitance of each individual MTJ can be accepted as $C_{s,p} = 118.8$ pF and $C_{s,ap} = 132.0$ pF for the parallel and anti-parallel states, respectively. The effective dielectric constant for MgO which is calculated from the single junction capacitances for both states is unphysically high compared to the bulk value for MgO $(\epsilon \cong 9.7\epsilon_0)$ [20]. However, in a single tunnel junction, the measured capacitance is the total capacitance with contribution of different capacitances such as the geometric capacitance due to insulator and interface capacitance due to interface states, surface roughness and charge accumulation and screening at the metal/insulator interfaces. In MTJs, in addition to these factors, a spin dependent screening potential at the interfaces because of the exchange bias has to be taken into account [5]. Therefore, measured capacitance can be described as:

$$\frac{1}{C} = \frac{1}{C_g} + \frac{1}{C_i} \tag{3}$$

where $C_g = \epsilon A/d$ is the geometric capacitance (A is the junction area, and d is the MgO thickness) and C_i is the interface capacitance. In multi junction arrays the layout of the junctions and geometry of their interconnections may cause different capacitive contributions. This makes it difficult to separate such a contribution from what we have referred to as interface capacitance in a single junction. These two contributions are therefore included together in the C_i-term in (3). With $A = 6.28\,\mu\mathrm{m}^2$, $\epsilon = 9.7\epsilon_0$ and $d = 1.7\,\mathrm{nm}$, we obtain $C_g = 0.317\,\mathrm{pF}$ for an individual MTJ. Upon inserting this value into (3), we find the interface capacitance densities of single junctions as $C_{\mathrm{id,p}} = -10.78$ and $C_{\mathrm{id,ap}} = -10.72\ \mathrm{pF}/\mu\mathrm{m}^2$ for parallel and anti-parallel states respectively. The negative interface capacitance is attributed to negative screening length due to excess pile-up of screening charge on the interface charges [21]. These results agree very well with the results reported earlier on AlOx [22] and MgO tunnel junctions [9], [23].

Although interface capacitance density results are similar, our results in general have important differences than other careful studies on frequency dependent impedance spectroscopy in magnetic tunnel junctions. One of the main differences is the sign of the tunneling magnetocapacitance. Our devices show positive magnetocapacitance (i.e. higher capacitance for anti-parallel and lower capacitance for parallel states) for positive magnetoresistance. However, positive TMR vs. negative TMC relationship has been reported for large area single tunnel junctions by several groups [9], [10] while zero TMC has been reported for single MTJs [23] which are comparable to the devices in this study in terms of single device area. Also, it is interesting to observe a significant TMC in array of junctions while comparable individual devices do not show any TMC. A possible explanation for this difference would be the serpentine structure. An AC signal with a wavelength short enough, could keep the MTJs on different arms of the serpentine at different potentials. Therefore an extra capacitance would exist in addition to geometric and interfacial capacitances. However, in our case, all the individual MTJs have the same potential since the wavelength of AC voltage is very long (up to 40 MHz ≈7.5 m

Authorized licensed use limited to: Brown University. Downloaded on March 24,2023 at 17:51:20 UTC from IEEE Xplore. Restrictions apply.

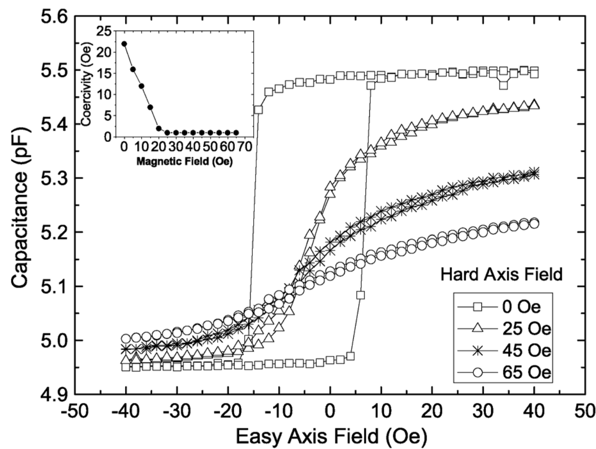

Fig. 7. TMC vs. easy axis field at 730 kHz for different hard axis fields. Inset: Coercivity vs. hard axis field.

in vacuum) compared to the dimensions of the sensor (less than a mm). Therefore we rule out this possibility for our devices. It is not an easy task to explain the microscopic origin of this magnetocapacitance difference because of complexity of our devices. Another important difference between our results and previous reports in the literature is the existence of the tunneling magnetoinductance. To our knowledge, there is no TML in MTJs reported previously. Traditionally, inductive components in circuit models for MTJs are attributed to the leads and wires in the junctions and electrical connections which are non-magnetic metals. They do not lead to any spin-inductance effect. As is the case for the magneto-capacitance we have observed, the microscopic origin of the magneto-inductance is not easy to explain with such complicated devices as our array junctions. There might be several factors playing a role for observing non-zero TML such as the current and magnetic field distribution in the meander lines or magnetic interactions between the individual MTJs and straight segments of the meander lines. Apart from these points, a possible shortcoming of the equivalent circuit model we used can also be leading to these results. Impedance spectroscopy should be performed at higher frequencies than our current limits (40 MHz) to evaluate this possibility. A systematic study of the sensors as a function of the number of individual junctions is required in order to resolve the TMC and TML differences we have observed in single junction devices [23] and junction arrays. These junctions should also be studied in terms of the geometry, by placing the MTJs on a straight line or on a meander lines with varying number of straight segments. The result of such a work will have significant importance on the application of the high frequency operation of MTJ magnetic field sensors since the magnetic field sensors include many individual MTJs connected to each other in order to increase the robustness and signal-to-noise ratio [24]. As we observed in our measurements, complex devices with many individual junctions do not necessarily reflect the characteristics of those of the individual devices they include.

Magnetic field sensing can also be performed via capacitive methods other than DC resistance measurements. Fig. 7 shows the evolution of extracted capacitance vs. magnetic field (easy axis) curves at 730 kHz as the bias field (hard axis) is changed. Capacitance values were calculated from (1). Measured DC resistance and $\mathrm{Re}(Z)$ values at 730 kHz were inserted into (1) for each external field along the easy axis and capacitance values were extracted. This procedure was repeated for each bias field in the hard axis direction from 0 to 65 Oe. Extracted capacitance values along with the DC resistance values were inserted into (2) and a visual fit to $\mathrm{Im}(Z)$ data was performed. L was used as a fit parameter for this step and we obtained very satisfactory results, confirming the reliability of the extracted capacitance. The results are given in Fig. 7. Only 4 of the capacitance vs. magnetic field curves (out of 14) are shown for clarity. The capacitance curve is hysteretic (multivalued function) with 22 Oe coercivity for zero hard axis field. As the hard axis field increased, the capacitance curve transforms into a single valued function (with $\approx$1 Oe coercivity) as is the case for the resistance curve. Compared to 40 Oe field at which the resistance curve becomes single-valued, capacitance curve reaches that point at 25 Oe. We calculated capacitive sensitivity in a similar way to resistive sensitivity; $1/C \times dC/dH$. The results are $10.2 \times 10^{-3}/\mathrm{Oe}$ and $2.1 \times 10^{-3}/\mathrm{Oe}$ between 25 and 65 Oe hard axis field values, respectively. Sensitivity decreases 1.7 to 4 times when spin dependent capacitance is used instead of resistance values.

IV. Conclusion

We have fabricated sensors based on MgO magnetic tunnel junction arrays which have micron scale single junctions connected in series. We performed DC magnetoresistance and frequency dependent AC-impedance spectroscopy measurements to find out the sensor response at high frequencies. We drove our devices into sensing mode by applying an external bias field and showed magnetic field sensing at high frequencies by using tunneling magnetocapacitance. We obtained high TMR and TMC values between 89.9 and 140.9% and 4.2 and 16%, respectively. It was shown that these values decrease as the devices gradually switch from memory mode to sensing mode. We have also shown that magnetocapacitance and magnetoresistance relationship in MTJs depends highly on the geometry of the device tested. We observed a positive relation between magnetoresistance and magnetocapacitance for our array-MTJ dvices, contrary to the reports on single MTJ devices in the literature. We attribute this difference to the geometry of the sensors studied in this report. Therefore, for the possible use of magnetocapacitance in sensing and other applications, it is crucial to characterize and extract the physical variables from complex impedance data for each case independently. Sensitivity of our devices decreased almost one order in capacitance measurements compared to resistance based sensing. However, sensing configuration was obtained earlier in capacitive sensing with respect to resistive sensing (25 vs. 40 Oe hard axis fields).

Acknowledgment

The authors would like to thank the Electrical Engineering department at the University of Iceland for use of their impedance analyzer. This research was funded by the Icelandic Research Fund and the University of Iceland Research Fund.

Authorized licensed use limited to: Brown University. Downloaded on March 24,2023 at 17:51:20 UTC from IEEE Xplore. Restrictions apply.

REFERENCES

[1] S. A. Wolf, D. D. Awschalom, R. A. Buhrman, J. M. Daughton, S. von Molnr, M. L. Roukes, A. Y. Chtchelkanova, and D. M. Treger, *Science*, vol. 294, pp. 1488–1495, 2001.

[2] X. Liu, C. Ren, and G. Xiao, "Magnetic tunnel junction field sensors with hard-axis bias field," *J. Appl. Phys.*, vol. 92, no. 8, pp. 4722–4725, 2002.

[3] G. Xiao and B. Schrag, "High resolution scanning magnetic microscope operable at high temperature," U.S. Patent 6,930,479, 2005.

[4] S. Ikeda, J. Hayakawa, Y. Ashizawa, Y. M. Lee, K. Miura, H. Hasegawa, M. Tsunoda, F. Matsukura, and H. Ohno, "Tunnel magnetoresistance of 604% at 300 K by suppression of Ta diffusion in CoFeB/MgO/CoFeB pseudo-spin-valves annealed at high temperature," *Appl. Phys. Lett.*, vol. 93, no. 8, p. 082508, 2008.

[5] S. Zhang, "Spin-dependent surface screening in ferromagnets and magnetic tunnel junctions," *Phys. Rev. Lett.*, vol. 83, no. 3, pp. 640–643, 2002.

[6] S. T. Chui and L. Hu, "AC transport in ferromagnetic tunnel junctions," *Appl. Phys. Lett.*, vol. 80, no. 2, pp. 273–275, 2002.

[7] G. Catalan, "Magnetocapacitance without magnetoelectric coupling," *Appl. Phys. Lett.*, vol. 88, p. 102902, 2006.

[8] K. T. McCarthy, A. Hebard, and S. B. Arnason, "Magnetocapacitance: Probe of spin-dependent potentials," *Phys. Rev. Lett.*, vol. 90, no. 11, p. 117201, 2003.

[9] P. Padhan, P. LeClair, A. Gupta, K. Tsunekawa, and D. D. Djayapawira, "Frequency-dependent magnetoresistance and magnetocapacitance properties of magnetic tunnel junctions with MgO tunnel barrier," *Appl. Phys. Lett.*, vol. 90, no. 14, p. 142105, 2007.

[10] H. Kaiju, S. Fujita, T. Morozumi, and K. Shiiki, "Magnetocapacitance effect of spin tunneling junctions," *J. Appl. Phys.*, vol. 91, no. 10, pp. 7430–7432, 2002.

[11] J. C. Huang and H. S. Hsu, "Complex capacitance spectroscopy as a probe for oxidation process of AlO [sub xpey1a]-based magnetic tunnel junctions," *Appl. Phys. Lett.*, vol. 85, p. 5947, 2004.

[12] A. M. Sahadevan, K. Gopinadhan, C. S. Bhatia, and H. Yang, "Parallel-leaky capacitance equivalent circuit model for MgO magnetic tunnel junctions," *Appl. Phys. Lett.*, vol. 101, p. 162404, 2012.

[13] Y. Lu, R. A. Altman, A. Marley, S. A. Rishton, P. L. Trouilloud, G. Xiao, W. J. Gallagher, and S. S. P. Parkin, "Shape-anisotropy-controlled magnetoresistive response in magnetic tunnel junctions," *Appl. Phys. Lett.*, vol. 70, no. 19, pp. 2610–2612, 1997.

[14] D. Lacour, H. Jaffres, F. Nguyen Van Dau, F. Petroff, A. Vaures, and J. Humbert, "Field sensing using the magnetoresistance of IrMn exchange-biased tunnel junctions," *J. Appl. Phys.*, vol. 91, p. 4655, 2002.

[15] S. van Dijken and J. M. D. Coey, "Magnetoresistance sensor with an out-of-plane magnetized sensing layer," *Appl. Phys. Lett.*, vol. 87, p. 022504, 2005.

[16] W. Skowroński, P. Wiśniowski, T. Stobiecki, S. Cardoso, P. P. Freitas, and S. van Dijken, "Magnetic field sensor with voltage-tunable sensing properties," *Appl. Phys. Lett.*, vol. 101, p. 192401, 2012.

[17] W. Shen, B. D. Schrag, A. Girdhar, M. J. Carter, H. Sang, and G. Xiao, "Effects of superparamagnetism in MgO based magnetic tunnel junctions," *Phys. Rev. B*, vol. 79, no. 1, p. 014418, 2009.

[18] X. Liu, D. Mazumdar, W. Shen, B. D. Schrag, and G. Xiao, "Thermal stability of magnetic tunneling junctions with MgO barriers for high temperature spintronics," *Appl. Phys. Lett.*, vol. 89, p. 023504, 2006.

[19] W. C. Chien, C. K. Lo, L. C. Hsieh, Y. D. Yao, X. F. Han, Z. M. Zeng, Y. T. Peng, and P. Lin, "Enhancement and inverse behaviors of magnetoimpedance in a magnetotunneling junction by driving frequency," *Appl. Phys. Lett.*, vol. 89, p. 202515, 2006.

[20] J. Fontanella, C. Andeen, and D. Schuele, "Low frequency dielectric constants of α quartz, sapphire, MgF_2, MgO," *J. Appl. Phys.*, vol. 45, p. 2852, 2002.

[21] H. M. Miesenböck and M. P. Tosi, "Exchange and correlation effects in the Visscher-Falicov model for metal intercalated graphite," *Z. Phys. B: Condens. Matter*, vol. 78, p. 255, 1990.

[22] G. Landry, Y. Dong, J. Du, X. Xiang, and J. Q. Xiao, "Interfacial capacitance effects in magnetic tunneling junctions," *Appl. Phys. Lett.*, vol. 78, no. 4, p. 501, 2001.

[23] S. Ingvarsson, M. Arikan, W. Shen, M. Carter, and G. Xiao, "Impedance spectroscopy of micron sized magnetic tunnel junctions with MgO tunnel barrier," *Appl. Phys. Lett.*, vol. 96, p. 232506, 2010.

[24] P. P. Freitas, R. Ferreira, S. Cardoso, and F. Cardoso, "Magnetoresistive sensors," *J. Phys.: Condens. Matter*, vol. 19, p. 165221, 2007.

Authorized licensed use limited to: Brown University. Downloaded on March 24,2023 at 17:51:20 UTC from IEEE Xplore. Restrictions apply.